The Application of Discontinuous Galerkin Space and Velocity Discretization to Model Kinetic Equations

Alexander Alekseenko[1], Natalia Gimelshein[2] and Sergey Gimelshein[2]

[1]Department of Mathematics, California State University Northridge, Northridge, California 91330, USA

[2]ERC, Inc, Edwards AFB, California 93524, USA

Abstract. An approach based on a discontinuous Galerkin discretization is proposed for the Bhatnagar-Gross-Krook model kinetic equation. This approach allows for a high order polynomial approximation of molecular velocity distribution function both in spatial and velocity variables. It is applied to model normal shock wave and heat transfer problems. Convergence of solutions with respect to the number of spatial cells and velocity bins is studied, with the degree of polynomial approximation ranging from zero to four in the physical space variable and from zero to eight in the velocity variable. This approach is found to conserve mass, momentum and energy when high degree polynomial approximations are used in the velocity space. For the shock wave problem, the solution is shown to exhibit accelerated convergence with respect to the velocity variable. Convergence with respect to the spatial variable is in agreement with the order of the polynomial approximation used. For the heat transfer problem, it was observed that convergence of solutions obtained by high degree polynomial approximations is only second order with respect to the resolution in the spatial variable. This is attributed to the temperature jump at the wall in the solutions. The shock wave and heat transfer solutions are in excellent agreement with the solutions obtained by a conservative finite volume scheme.

1. Introduction

Over the last decade, numerical modeling of flows in gas-driven micro- and nanoscale devices has drawn much attention due to its application to sensors, actuators, filters, pumps, flow control systems, and so forth. For many of these devices, development stems from trial and error approaches fitted around device fabrication. For their development to take a leap forward, accurate and efficient numerical modeling is necessary in areas where flow diagnostics may be limited or impossible. The choice and use of the numerical approach suitable to microscale flows is primarily related to a number of fluid dynamic effects peculiar to these flows. These effects, such as velocity slip, temperature jump, thermal creep, and viscous heating, dominate in many microdevices based on microelectromechanical technologies. Due to the small characteristic dimensions of microscale flows—typically on the order of tenths of micrometers to millimeters—heat conductivity and diffusivity play a very important role. Large surface-to-volume ratios imply that gas-surface interactions are very important. The gas mean free paths

are comparable to characteristic flow dimensions, which results in significant deviation from equilibrium. This means that in many cases conventional computational fluid dynamics methods such as the solution of Navier-Stokes equations are not applicable. Instead modeling must be based on kinetic gas theory.

Kinetic gas theory describes gas properties through the distribution function of molecular velocities. The governing equation for the velocity distribution function is the Boltzmann equation. It expresses the variation of the distribution function due to molecular free flight, action of external forces and intermolecular collisions. For a single species monatomic gas, the Boltzmann equation has the form

$$\frac{\partial f}{\partial t} + \vec{u}\frac{\partial f}{\partial \vec{x}} + \frac{\vec{X}}{m}\frac{\partial f}{\partial \vec{u}} = \int (f' f_1' - f f_1) g b \, \mathrm{d}b \, \mathrm{d}\varepsilon \, \mathrm{d}\vec{u_1}, \tag{1}$$

where the velocity distribution function f is defined by the condition that $f(t, \vec{x}, \vec{u}) \, \mathrm{d}\vec{x} \, \mathrm{d}\vec{u}$ is the number of molecules at time t with velocities between $\vec{u}$ and $\vec{u} + \mathrm{d}\vec{u}$ and coordinates between $\vec{x}$ and $\vec{x} + \mathrm{d}\vec{x}$. Here, $\vec{X}$ is the external force, $g = |\vec{u} - \vec{u_1}|$ is the magnitude of relative velocity of colliding molecules, and b and ε are geometric impact parameters.

The Boltzmann equation is a nonlinear integro-differential equation amenable to analytical solution only for a small number of special cases of collisionless or spatially homogeneous problems. Difficulties encountered in numerical solution of the Boltzmann equation are primarily attributed to the multidimensional phase space—physical coordinates and velocity coordinates—and the multidimensional collision integral in the right-hand side. For three-dimensional flows of monatomic gases the collision integral involves integration over a five-dimensional domain. This limits the direct numerical integration of the Boltzmann equation [1] to simplified collision models, such as hard sphere molecules, and one- and two-dimensional flow problems. The molecular dynamics method [2] is also applicable to the solution of the Boltzmann equation, but it is even more limited in terms of flow dimensionality and problem size. The most powerful and widely used approach to the solution of the Boltzmann equation is currently the direct simulation Monte Carlo (DSMC) method [3].

Although the DSMC method is more efficient than the two former approaches, it still suffers from high computational cost compared to conventional continuum CFD methods. The computational cost limitation of the DSMC method are especially severe at low Knudsen numbers; in many cases it makes this method an unacceptable choice. This is the case for three-dimensional low speed flows where the computational cost is impacted by flow dimensionality, the long time to reach steady state, the low signal-to-noise ratio, multiple physical scales and other factors.

There are several alternative DSMC-based approaches proposed to deal with the problem of low signal-to-noise ratio that allow reduction in macroparameter sampling time compared to the standard DSMC method [4, 5, 6, 7]. Although all these techniques significantly reduce steady-state time averaging cost, they do not deal with the computational cost associated with long times to reach steady state typical for low speed micro- and nanoscale flows. This time is usually comparable with or larger than the time needed to sample macroparameters, and thus any attempt to shorten the latter is bounded by the former. In addition, these methods do not address the problem of particle correlations and related solution accuracy, peculiar for particle methods and

greatly amplified for low-speed flows. Finally, particle approaches are poorly suited for unsteady fluid-thermal coupling due to extremely high statistical scatter of instantaneous ensemble-averaged heat fluxes from gas to surface.

This means that current applications of particle-based, statistical approaches to the solution of the Boltzmann equation for modeling low-speed microscale gas flows are fairly limited. A plausible numerical alternative is a deterministic solution of several available simplified forms of the Boltzmann equation, known as model kinetic equations. Two of the most known model kinetic equations, the Bhatnagar-Gross-Krook (BGK) [8] and the ellipsoidal statistical (ES) [9] kinetic models, use a non-linear relaxation term instead of the full Boltzmann collision integral. In spite of the simpler collision term, both models possess the same collision invariants as the Boltzmann equation.

The main objective of this work is to present a new approach to the solution of the BGK model kinetic equation based on a Galerkin discretization of both physical and velocity space and to analyze its applicability to model microscale gas flows. Advantages and disadvantages of the discontinuous Galerkin (DG) method of solution of model kinetic equations are discussed. For two classical problems of rarefied gas dynamics—normal shock wave and heat transfer between parallel plates—the DG solutions are compared with the solutions obtained by a finite volume (FV) approach.

2. Challenges of the numerical solution of the BGK equation

The BGK equation is a kinetic model obtained from an intuitive simplification of the collision integral in the Boltzmann equation. Similar to the Boltzmann equation, it is solved for the multi-dimensional molecular velocity distribution function. In the BGK model the collision operator is replaced with a simpler operator

$$\nu(f_0 - f),$$

where $\nu(t, \vec{x})$ is the collision frequency and $f_0(t, \vec{x})$ is the Maxwellian equilibrium distribution function

$$f_0 = n(t, \vec{x})(2\pi RT(t, \vec{x}))^{-3/2} \exp\Big(-\frac{(\vec{u} - \vec{\vec{u}}(t, \vec{x}))^2}{2RT}\Big). \tag{2}$$

The gas density, n, bulk velocity, $\vec{\vec{u}}$ and temperature, T, are defined as follows:

$$\begin{aligned} n(t, \vec{x}) &= \int_{\mathbb{R}^3} f(t, \vec{x}, \vec{u}) d\vec{u}; \\ n(t, \vec{x})\vec{\vec{u}}(t, \vec{x}) &= \int_{\mathbb{R}^3} \vec{u} f(t, \vec{x}, \vec{u}) d\vec{u}; \\ n(t, \vec{x})T(t, \vec{x}) &= \frac{1}{3R} \int_{\mathbb{R}^3} (\vec{u} - \vec{\vec{u}})^2 f(t, \vec{x}, \vec{u}) d\vec{u}, \end{aligned} \tag{3}$$

where R is the gas constant. The BGK model satisfies the mass, momentum, and energy conservation laws and the Boltzmann's H-theorem expressing the increase of entropy of the gas under consideration. Kinetic models should also reproduce the gas transport coefficients—viscosity, thermal conductivity and species diffusivity—resulting from the Boltzmann equation. The primary advantage of this numerical alternative is its relatively high computational efficiency. Previous application of the solution of the model kinetic equations to low-speed microscale gas flows showed an

improvement in numerical efficiency of more than two orders of magnitude using a deterministic solution of model kinetic equations was used instead of the DSMC method [10, 11].

Current approaches to the solution of model kinetic equations include either finite difference [10] or, much more frequently, finite volume methods [12, 13, 14]. Finite volume approaches are generally more robust and may be applied to complex two- and three-dimensional geometries. There is also a methodology that enforces conservation laws [12]. However, there are several problems related to the application of finite volume approaches to model low-speed microflows. First, their efficiency, while much higher than that of DSMC, is still much lower than the efficiency of continuum CFD solvers. This is primarily related to the multi-dimensionality of the velocity distribution function which depends on three spatial coordinates and three components of velocity. The existing finite volume solvers for model kinetic equations are typically second order in physical space. Their approximation in velocity space is generally based on piecewise constant functions, also known as the discrete ordinate approach. As a result, a large number of velocity bins and spatial cells is usually needed to obtain a converged solution. This significantly limits the application of these solvers to three-dimensional flows with a considerable degree of non-equilibrium.

The second problem is related to virtual cells behind the surface that are necessary in the implementation of finite volume schemes. The use of such cells impacts the accuracy of calculation of fluxes at gas-solid interfaces. Errors caused by the use of virtual cells not only affect gas properties near the surface, but also propagate into the gas volume. The property affected most is the gas velocity. An example of undesirable numerical effects induced by virtual cells is given in Figure 1, where the x velocity and streamlines are shown around a radiometer vane immersed in a 6 Pa argon gas and heated to 415 K on the left side and 395 K on the right side. The radiometer is centered at $(0, 0)$. The lower boundary is the symmetry plane, and the other boundaries are chamber walls kept at 300 K. It is seen that near the chamber walls there are finite (about 0.1 m/s) flow velocities in the direction normal to the wall. These artificial velocities clearly change the shape of the large vortex surrounding the vane and affect the radiometric force prediction.

The third potential problem is the lack of mass, momentum and energy conservation in implicit finite volume schemes and the need to use a special technique to impose conservation in explicit schemes. The issues related to the conservation laws may be amplified in transient flows for which accurate prediction of time-dependent properties is a necessity.

One possible way to address the above problems is to use a DG type of discretization both in physical and velocity space. High order DG schemes are generally formulated both for regular and irregular partitions. They have compact stencils and are well suited for adaptive grid refinement. A weak enforcement of fluxes in DG discretizations is well suited for implementing realistic gas-surface interaction models. In particular, it does not require the use of virtual cells behind solid interfaces. This type of discretization will generally allow one to drastically increase the order of discretization and thus reduce computational time in multi-dimensional problems. A DG approach is therefore used in this work.

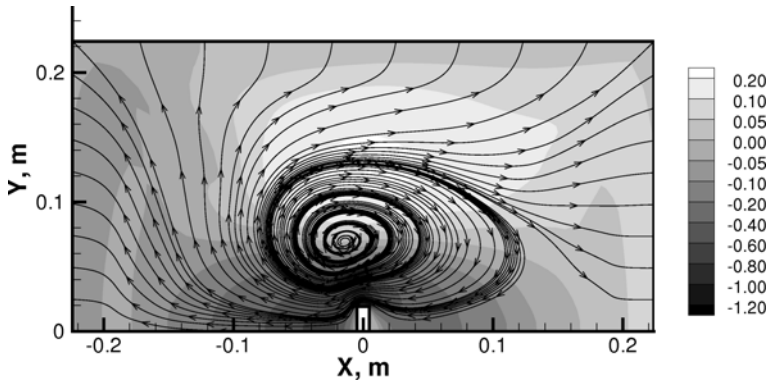

FIGURE 1. Flow velocity and streamlines around a radiometer vane in a 6 Pa argon gas, obtained by a finite volume approach to the BGK equation.

Recently an application of DG discretizations to the Boltzmann equation was discussed in [21, 18]. In [19], the ellipsoidal-statistical BGK equation is solved using a DG discretization in the spatial variable and discrete ordinates in the velocity variable. In this paper high order DG discretizations in the spatial variable are augmented by high order DG discretizations in the velocity variable.

A high order DG discretization in the velocity variable is expected to provide sufficient accuracy to enforce conservation of mass, momentum and energy with no additional effort. It is also important to compare solutions obtained by high order DG velocity discretizations with the conservative discretization [12]. Both steady-state and transient flow solutions are of interest.

3. The discontinuous Galerkin discretization

Discontinuous Galerkin methods have been applied to different gas dynamic equations in the past. A theoretical study of the convergence and stability of DG formulations for the Boltzmann equation was conducted in [17]. A general description and theory of Runge-Kutta DG methods may be found in [23, 22]. The first application of a DG discretization of the BGK equation in both spatial and velocity variables was presented in [20]. As in [20] only approximations with finite support are used in this work. Let us consider a finite region $\Upsilon \subset \mathbb{R}^3$ in the velocity space and assume that the distribution function $f(t, \vec{x}, \vec{u})$ and its integrals are small in $\mathbb{R}^3 \setminus \Upsilon$. Note that the method can be extended to infinite domains by using a mixture of finite and infinite elements with appropriate basis functions.

Let us introduce partitions of the spatial domain $\Omega \in \mathbb{R}^3$ into polyhedral elements K_j, $j = 1, \ldots, N$ and velocity domain Υ into polyhedral elements V_i, $i = 1, \ldots, M$. Let polynomial basis functions $\varphi_{p,j}(\vec{x})$, $p = 1, \ldots, k$ and $\lambda_{l,i}(\vec{u})$, $l = 1, \ldots, s$ be defined on K_j and V_i, respectively. On each phase element $K_j \times V_i$ the solution is sought in the form

$$f(t, \vec{x}, \vec{u})|_{K_j \times V_i} = \sum_{l=1}^{s} \sum_{p=1}^{\mu(l)} f_{l,i;p,j}(t) \varphi_{p,j}(\vec{x}) \lambda_{l,i}(\vec{u}). \tag{4}$$

If $\lambda_{l,i}(\vec{u})$ are polynomials of degree not greater than s and $\varphi_{p,j}(\vec{x})$ are polynomials of degree not greater than k, then an efficient discretization is obtained by setting $\mu(l) = \min(\texttt{max\_degree} - l, k)$, where `max_degree` is the desired maximum degree of (4). In this paper $\texttt{max\_degree} = \max(k, s)$.

Let us substitute (4) into (1) and multiply the result by a basis function $\lambda_{m,i}(\vec{u})$, $m = 1, \ldots, s$. The DG discrete velocity formulation is obtained by successive integration over V_i as follows:

$$\begin{aligned} &\partial_t \mathbf{f}_{ij}(t,\vec{x}) + \partial_x \hat{\mathbf{T}}_i^u \mathbf{f}_{ij}(t,\vec{x}) + \partial_y \hat{\mathbf{T}}_i^v \mathbf{f}_{ij}(t,\vec{x}) + \partial_z \hat{\mathbf{T}}_i^w \mathbf{f}_{ij}(t,\vec{x}) \\ &\qquad = \nu\Big((\mathbf{D}_i)^{-1} \int_{V_i} f_0 \lambda_{m,i} - \mathbf{f}_{ij}(t,\vec{x})\Big). \end{aligned} \tag{5}$$

Here $\mathbf{f}_{ij}(t,\vec{x}) := \sum_{p=1}^{\mu(l)} f_{l,i;p,j}(t)\varphi_{p,j}(\vec{x})$ is the vector of coefficients of the DG discrete velocity representation and square matrices $\hat{\mathbf{T}}_i^v = (\mathbf{D}_i)^{-1}\mathbf{T}_i^v$, $\hat{\mathbf{T}}_i^u = (\mathbf{D}_i)^{-1}\mathbf{T}_i^v$ and $\hat{\mathbf{T}}_i^w = (\mathbf{D}_i)^{-1}\mathbf{T}_i^v$ represent the coefficients of the DG discrete velocity formulation. Matrix multiplication notation is used in (5) so that $\hat{\mathbf{T}}_i^u \mathbf{f}_{ij} = \sum_{l=0}^{s} \hat{T}_{ml,i} f_{l,ij}$. Also,

$$\begin{aligned} T^u_{ml,i} &= \int_{V_i} u\lambda_{l,i}\lambda_{m,i}, \quad T^v_{ml,i} = \int_{V_i} v\lambda_{l,i}\lambda_{m,i}, \\ T^w_{ml,i} &= \int_{V_i} w\lambda_{l,i}\lambda_{m,i}, \quad D_{ml,i} = \int_{V_i} \lambda_{l,i}\lambda_{m,i}. \end{aligned} \tag{6}$$

In order to derive the spatial discretization, (6) is multiplied by a basis function $\varphi_{q,j}(\vec{x})$, $q = 1, \ldots, \mu(m)$ and integrated over K_j, resulting in

$$\begin{aligned} &\sum_{p=1}^{\mu(m)} \partial_t f_{m,i;p,j}(t) C_{pq,j} - \sum_{l=1}^{s} \hat{T}^u_{ml,i} \sum_{p=1}^{\mu(l)} f_{l,i;p,j}(t) C^x_{pq,j} \\ &\quad - \sum_{l=1}^{s} \hat{T}^v_{ml,i} \sum_{p=1}^{\mu(l)} f_{l,i;p,j}(t) C^y_{pq,j} - \sum_{l=1}^{s} \hat{T}^w_{ml,i} \sum_{p=1}^{\mu(l)} f_{l,i;p,j}(t) C^z_{pq,j} \\ &\quad + \sum_{l=1}^{s} \mathcal{L}^-_{ml,ij} \sum_{p=1}^{\mu(l)} f_{l,i;p,j^*}(t) C^{\partial K}_{pq,j^*} + \sum_{l=1}^{s} \mathcal{L}^+_{ml,ij} \sum_{p=1}^{\mu(l)} f_{l,i;p,j}(t) C^{\partial K}_{pq,j} \\ &\quad = \int_{\partial K_j} \nu\Big[\Big(\sum_{l=1}^{s} (D_{ml,i})^{-1} \int_{V_i} f_0 \lambda_{l,i}\Big) - \sum_{p=1}^{\mu(m)} f_{m,i;p,j}(t)\varphi_{p,j}\Big]\varphi_{q,j}, \end{aligned} \tag{7}$$

where

$$\mathbf{C}_j = C_{pq,j} = \int_{K_j} \varphi_{p,j}(\vec{x})\varphi_{q,j}(\vec{x}),$$

$$\mathbf{C}^x_j = C^x_{pq,j} = \int_{K_j} \varphi_{p,j}(\vec{x})\partial_x\varphi_{q,j}(\vec{x}),$$

$$\mathbf{C}^y_j = C^y_{pq,j} = \int_{K_j} \varphi_{p,j}(\vec{x})\partial_y\varphi_{q,j}(\vec{x}),$$

$$\mathbf{C}^z_j = C^z_{pq,j} = \int_{K_j} \varphi_{p,j}(\vec{x})\partial_z\varphi_{q,j}(\vec{x}),$$

$$\mathbf{C}^{\partial K}_j = C^{\partial K}_{pq,j} = \int_{\partial K_j} \varphi_{p,j}(\vec{x})\varphi_{q,j}(\vec{x})d\sigma,$$

$$\mathbf{C}^{\partial K}_{j^*} = C^{\partial K}_{pq,j^*} = \int_{\partial K_j} \varphi_{p,j^*}(\vec{x})\varphi_{q,j}(\vec{x})d\sigma. \tag{8}$$

An upwind flux is used in this formulation. Thus j^* is the index corresponding to the element K_{j^*} that shares the particular part of the boundary with K_j. Projection operators $\mathcal{L}^+_{lm,ij}$ and $\mathcal{L}^-_{lm,ij}$ appearing in (7) separate modes in $\mathbf{f}_{ij}$ that propagate inside and outside K_j, respectively. They are defined as follows. Let λ_l and $\vec{\xi}_l$, $l = 1, \ldots, s$ be the eigenvalues and the corresponding eigenvectors of $\hat{\mathbf{T}}^n_{ij}$, respectively. Let $\mathbf{A}_{ij}$ be the matrix whose l-th column is $\vec{\xi}_l$. We define the diagonal matrices

$$\Lambda^- = \mathrm{diag}\,(\min(0,\lambda_1), \ldots, \min(0,\lambda_s)),$$
$$\Lambda^+ = \mathrm{diag}\,(\max(0,\lambda_1), \ldots, \max(0,\lambda_s)).$$

Then the projection operators are given by

$$\mathcal{L}^-_{ij} = \mathbf{A}_{ij}\Lambda^-\mathbf{A}^{-1}_{ij}, \quad \mathcal{L}^+_{ij} = \mathbf{A}_{ij}\Lambda^+\mathbf{A}^{-1}_{ij}.$$

A one-dimensional DG code has been developed that incorporates the above scheme. The application of the code to the shock wave and heat transfer problems is discussed in the following sections.

4. The normal shock wave problem

The accuracy and convergence of the DG approach (8) is examined below in application to the solution of the normal shock wave problem. This is a classical problem of gas dynamics: as such it was used for accuracy and applicability analysis of a large number of numerical methods of fluid dynamics. The normal shock wave problem is characterized by a significantly non-equilibrium velocity distribution function. It allows one to avoid problems associated with boundary conditions at solid walls. In this paper, a weak shock wave in argon gas was modeled for a Mach number of 1.2 and an upstream number density and temperature of 1.6×10^{21} molecule/m^3 and 300 K, respectively. The argon viscosity was assumed to be 2.117^{-5} N·s/m^2 at 273 K. The length of the computational domain was 0.2 m, which amounts to about 300 upstream mean free paths. This is large enough to avoid the impact of the size of the computational domain.

The results obtained by the DG approach are compared with the solution of the BGK equation obtained by the finite volume approach. (Analysis of the accuracy of the BGK approximation to the Boltzmann equation for the normal shock wave problem and comparison with other kinetic approaches is not the topic of the present work and may be found elsewhere [15].) A finite volume 2D/axisymmetric code SMOKE [16] has been used to solve the BGK equation. SMOKE is a parallel code based on conservative numerical schemes developed by L. Mieussens [12]. A second order spatial discretization is used along with explicit time integration. One thousand spatial cells were used, with specular boundaries set to model 1D flow in the longitudinal direction. The convergence study on the velocity grid was conducted, with the number of (x, y, z) velocity points ranging from (20,10,10) to (60,40,40). The results for the (30,40,40) grid are presented below.

Figure 2 shows the comparison of the solutions obtained by two different approaches to the model kinetic equation. The DG solution was obtained by fourth degree polynomial approximations in space on 64 cells and eighth degree polynomial approximations in velocity space on 32 velocity bins. A Runge-Kutta explicit scheme was used for the time integration. Only a part of the computational domain is presented in order to show more detail of the shock wave structure. The normalized macroparameters, $\mathrm{U} = \frac{U-U_{-\infty}}{U_{+\infty}-U_{-\infty}}$ and $\mathrm{T} = \frac{T-T_{-\infty}}{T_{+\infty}-T_{-\infty}}$, are shown. Hereafter the DG solution is denoted by BGK-DG and the finite volume solution is denoted by BGK-FV. The results show very good agreement between the two approaches which may be considered to be a verification of the developed DG code.

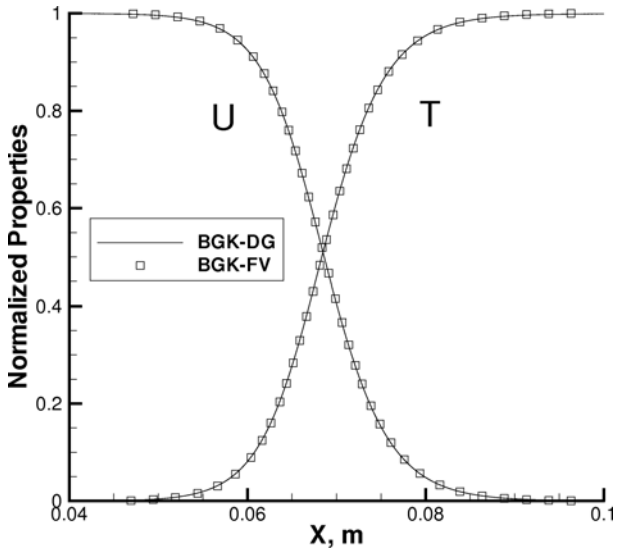

FIGURE 2. Normalized velocity and temperature in a Mach 1.2 shock wave. Comparison between the DG and FV approaches.

High order convergence of the DG method is illustrated in Figures 3 and 4. Figure 3 shows the convergence of density profiles with respect to the velocity variable for different orders of the DG velocity approximation. Hereafter, the relative error is

calculated as $|\rho - \rho_{ref}|/\rho$, where ρ is the gas density in the current solution and ρ_{ref} is the gas density in a reference solution. Solutions in Figure 3(a) are computed using DG approximations by first degree polynomials, Figure 3(b) by fourth degree polynomials and those on Figure 3(c) by eighth degree polynomials. The DG discretization in x is the same in each case and used fourth degree polynomials on 32 cells. Integration in time was conducted by a fifth order Runge-Kutta method. Note that using different numbers of spatial and velocity cells resulted in sightly different steady-state location of the shock wave profile. The graphs were therefore obtained by translating density profiles that correspond to different cell numbers so that they coincided in the center of the shock wave where the normalized density was equal to 0.5. The accuracy of translation was maintained to the eleventh digit. This explains the sharp drop in the numerical error in the center of the shock wave. Note that the reference solutions ρ_{ref} in Figures 3(a)–(c) are different in each case and were obtained using the same order of velocity discretization as the compared solutions but on finer velocity grids. Specifically, first degree polynomials on 512 velocity bins were used as reference values in Figure 3(a), fourth degree on 128 bins in Figure 3(b) and eighth degree on 64 bins in Figure 3(c). This allows one to show that the solutions converge with respect to the resolution in u in each case. Moreover, the graphs do not change significantly if the reference solutions in Figures 3(a) and (b) are replaced by the solution obtained by the eighth degree polynomials on 64 bins used in Figure 3(c). It may therefore be concluded that the solutions do converge to an approximate solution corresponding to a given discretization in x. At the same time, comparison to a solution obtained on a finer grid in x—for example, 64 spatial cells—shows loss of convergence below the level of 10^{-6} at the center of the shock wave, as illustrated in Figure 3(d). This suggests that the numerical errors in these solutions are dominated by the errors of discretization in the spatial variable. In particular, no significant improvement in the solution can be achieved by further velocity mesh refinement.

The shock wave solutions examined in Figure 3 exhibit very fast convergence above the 10^{-6} level. Indeed, Figures 3(a) and (b) show an improvement in the solution accuracy that is seemingly better than the order of the polynomial approximation used. This convergence can be attributed to the properties of the distribution function. It is known that the error of evaluating the integral $\int_{-\infty}^{\infty} e^{-u^2} du$ by the trapezoidal rule on a sufficiently large finite interval decreases faster than any power of the mesh size. Similarly fast convergence of quadrature rules is expected for all smooth functions that rapidly decrease at infinity. It is believed that the fast convergence of the macroparameters with respect to the resolution in velocity space is due to the exponential decrease of the distribution function. The fast convergence is not limited to high order DG approximations. It is expected to hold for the discrete ordinate approach on uniform velocity bins as well. The other necessary condition for fast convergence is the smoothness of the solution. In particular, one should not expect fast convergence in velocity space if the solution is contaminated by errors of discretization in physical space. Note that the convergence becomes only second order in Figure 3(b) once the numerical error had reached the level of the error of spatial discretization. Interestingly, eighth degree polynomial approximations are much less sensitive to the roughness of the solution and

converge to almost the round-off level.

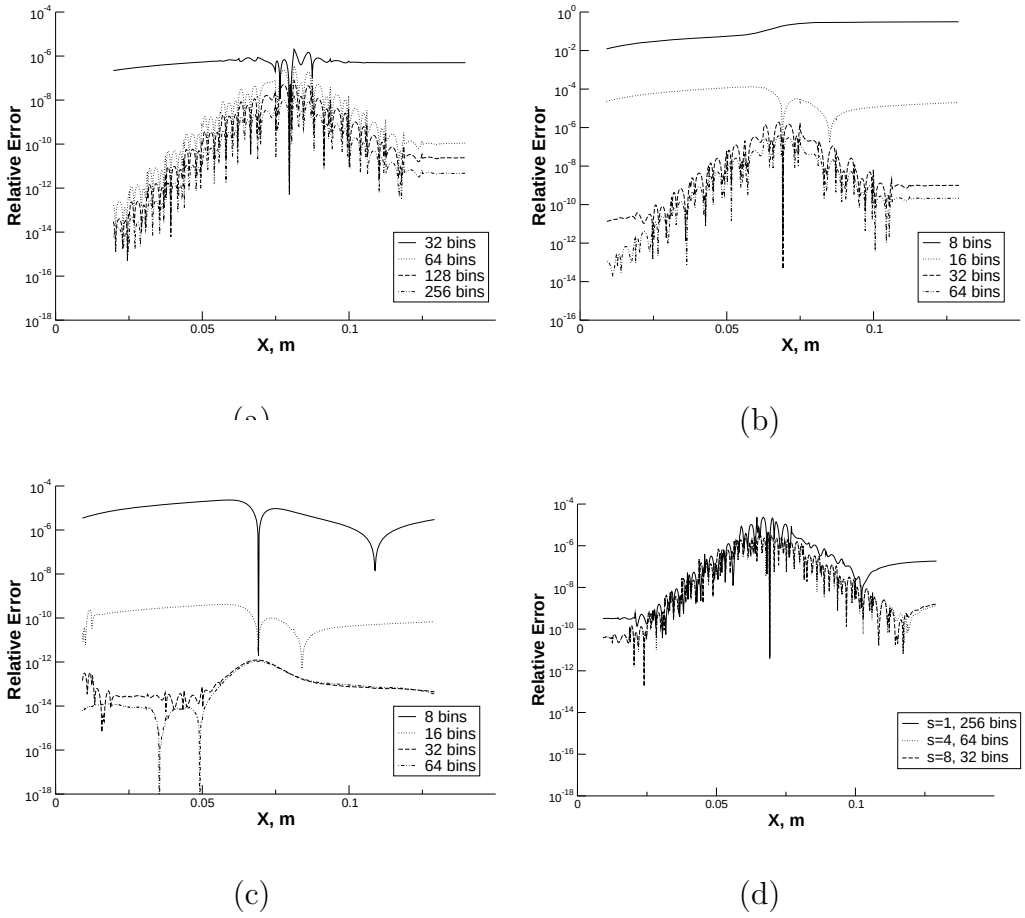

FIGURE 3. Convergence of the DG solution in a Mach 1.2 shock wave as a function of the number of velocity bins. Comparison of the DG discretizations by (a) first, (b) fourth and (c) eighth degree polynomials. In figure (d) solutions on 32 spatial cells are compared to a solution on 64 spatial cells.

The CPU times that correspond to the simulations shown in Figure 3 are given in Table 1. The results were obtained on an AMD Opteron 252 processor. Analysis of the Table 1 and Figure 3 shows that it is impractical to use more than 64 bins in the first degree, 32 bins in the fourth degree and 16 bins in the eighth degree polynomial approximations. Thus the required CPU times are $13,060$ seconds for $s = 1$, $15,486$ seconds for $s = 4$, and $15,757$ seconds for $s = 8$. While these run times are comparable, the $s = 8$ solution may be preferred since it has a faster convergence.

Figure 4 illustrates the convergence of the density profile with respect to the spatial variable. Two cases of DG approximation in physical space are shown, with first degree polynomials plotted in Figure 4(a) and fourth degree polynomials in Figure 4(b). The temporal Runge-Kutta integration is second and fifth order, respectively. The DG velocity discretization is conducted using eighth degree polynomials on 32 uniform

$s=1$		$s=4$		$s=8$	
M	t, CPU sec.	M	t, CPU sec.	M	t, CPU sec.
32	6,349	8	3,891	8	7,713
64	13,060	16	7,683	16	15,757
128	25,232	32	15,486	32	30,117
256	49,665	64	30,579	64	61,188

TABLE 1. CPU time as a function of degree of polynomial approximation in the velocity space.

velocity bins in each case. Note that the scheme using fourth order polynomials exhibits considerably less oscillation and has better convergence at the center of the shock wave. In both cases, the convergence generally corresponds to the order of the polynomial approximation used.

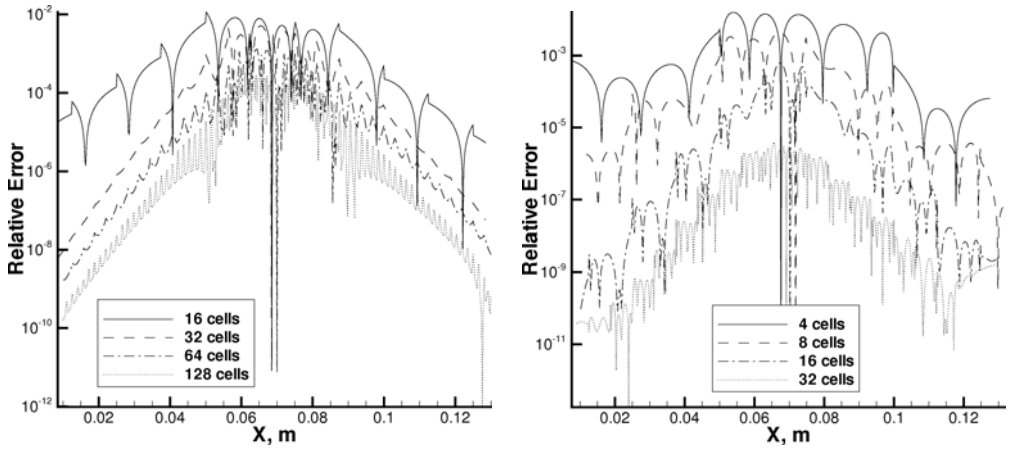

(a) (b)

FIGURE 4. Convergence of density in a Mach 1.2 shock wave as a function of spatial cells. Comparison of (a) second and (b) fifth order DG discretizations.

The presented results show that the DG discretization produces accurate solutions that converge with high order both in physical and velocity variables. Note also that since high order discretization in velocity space does not lower the CFL condition for the temporal discretization, it may serve as an inexpensive way to increase solution accuracy.

Implementation of the DG procedure for the velocity and physical space discretizations is more cumbersome than that of a typical FV approach. As a result, computational time for the DG method is larger than that of FV methods with the same order of discretizations. In the case of the second order in space and first order in velocity discretizations the FV solver SMOKE was two to three times faster than the DG code. Performance of the DG method, however, can be improved by increasing the order of polynomial approximation.

Table 2 shows the maximum error near the center of the shock wave and the CPU time used for simulations shown in Figure 4. It can be seen that the simulations that use a piece-wise linear approximation in space converge to $\sim 10^{-4}$ for 128 cells. At the same time, similar error is achieved for only 16 cells when a fourth degree polynomial approximation is used. Comparison of computational times shows that the high order method is about 3.77 times faster. Table 2 also suggests that more accurate simulations will require considerably longer time for low order techniques. At least four additional grid refinements are necessary for the piece-wise linear simulations to achieve 10^{-6} accuracy. Since each refinement results in about 3.5 increase in CPU time, simulations based on first degree polynomial approximations will be at least 150 times slower than those for fourth degree approximations. Performance of the DG method (7) may be

$k=1$			$k=4$		
N	rel. err.	t, CPU sec.	N	rel. err.	t, CPU sec.
16	8.2E-3	985.97	4	1.3E-2	876.09
32	4.1E-3	3264.48	8	3.8E-3	3151.16
64	1.0E-3	11551.34	16	4.1E-4	11825.48
128	1.2E-4	44593.05	32	2.2E-6	45416.36

TABLE 2. CPU times for simulations by second order and fifth order methods shown on Figure 4.

further improved by careful selection of basis functions and quadrature formulas for the evaluation of moments of the distribution function. One way to do that is to generalize the approach of [21] to the DG methods and use Lagrange polynomials on Hermite nodes as velocity basis functions. The advantage of such a basis is that matrices (6) are diagonal. This will simplify implementation and reduce computational time.

5. Heat transfer between parallel plates

The normal shock wave problem, while being important for testing the method applicability and convergence for gas flow modeling, does not allow one to analyze the approach accuracy and robustness for modeling gas-solid interfaces. However, gas-surface interactions are extremely important for low-speed gas flows in microscale devices where reliable modeling of such interactions is indispensable. The Maxwell model of gas-surface collisions and, in particular, collisions with full momentum and energy accommodation at the surface (fully diffuse reflection) are most widely used in computations of microscale gas flows at the kinetic level. The Maxwell model is naturally suitable for particle approaches such as DSMC. Deterministic kinetic methods, both finite difference and finite volume, generally suffer from the loss of accuracy related to the discontinuity in the molecular velocity distribution function at the surface. An exception here is the fully specular reflection, which is not physically realistic.

In order to study the affect of gas-surface interactions on accuracy and convergence of the DG approach, a one-dimensional heat transfer between parallel plates was considered, with fully diffuse reflection assumed at the wall. The cold and hot wall temperatures were 300 K and 1000 K, respectively. Argon gas was modeled for two Knudsen numbers, $Kn = 0.01$ and 1.

First, we examine the conservation of the total mass in the numerical solution. In the previous section it was concluded that low order velocity discretization methods may provide accurate estimates of moments if the numerical solution is sufficiently smooth. While this conclusion is true for the shock wave problem, it is not the case for the heat transfer problem. Figure 5 shows the relative error in the total mass of the gas between the plates as a function of time. Solutions obtained by fourth and eighth degree polynomial approximations in velocity are shown in Figures 5(a) and (b), respectively. The spatial DG discretization is by fourth degree polynomials with 32 spatial cells in both cases.

As expected, the error in the total mass decreases as the number of velocity bins increases. However the rate of decrease suggests that for a fifth order polynomial approximation the decrease in error is only of second order. At the same time, the eighth degree polynomial approximation shown on Figure 4(b) conserves mass within the ninth digit even when only 16 velocity bins are used. Note that the rate of convergence is lost below the 10^{-9} level. However, at this point, the simulations had reached the rounding off error limit and any further improvement is not expected. Note that the use of eighth degree polynomial approximations also allows one to conserve energy flux and maintain zero mass and momentum fluxes at the 10^{-8} level of accuracy throughout the computational domain.

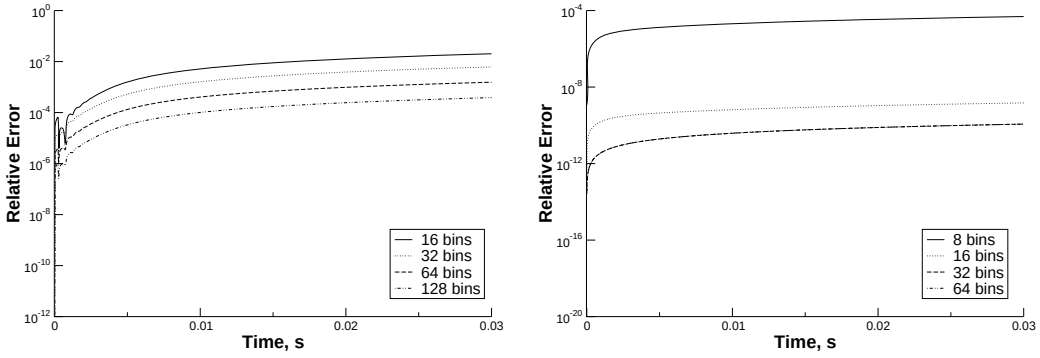

(a) (b)

FIGURE 5. Convergence of relative error in the total mass with respect to the resolution in velocity space. Comparison of (a) fourth and (b) eighth degree polynomial approximations.

Similar observations can be made regarding the convergence of the density profile with respect to the velocity variable. Comparison of solutions obtained by fourth and eighth degree polynomial approximations in velocity space is given in Figure 6. The cold wall is located at $x = 0$ and the hot wall is located at $x = 0.1$. As seen in Figure 6(a) the solutions obtained by the fourth degree approximation converge with the third order or more slowly. As in the mass conservation analysis, the order of convergence is two units less than the order of polynomial approximation used. It is reasonable to assume that the convergence is slower because the solution is not

sufficiently smooth (the reasons for this are discussed below). At the same time, the results obtained using eighth degree polynomials shown in Figure 6(b) are not sensitive to the non-smoothness of the solution and quickly converge to the level of the round-off error.

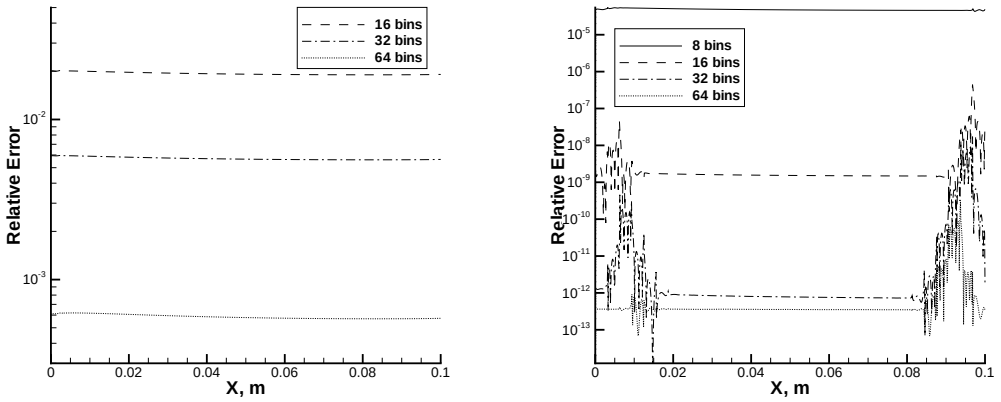

(a) (b)

FIGURE 6. Convergence of the solution in a Kn=0.01 heat transfer problem as a function of the number of velocity bins. Comparison of (a) fourth and (b) eighth degree polynomial DG approximation in velocity space.

It is not immediately obvious why the solution looses its smoothness in the entire domain. A study of convergence with respect to the resolution in physical space suggests that the non-smoothness is caused by the diffuse boundary conditions. The convergence of the density profile with respect to the resolution in physical space is shown in Figure 7, where solutions obtained using first and fourth degree polynomial DG approximations in x are shown. The Runge-Kutta time integrations are second and fifth order, respectively. The discretization in velocity space is conducted on 32 velocity bins using eighth degree polynomials for both cases. The order of convergence for the density profile is second order at best. Also, there is an oscillation near the walls. We believe that the reason for this is the discontinuity in the velocity distribution function near the wall, as is explained below.

Generally the solution to the heat transfer problem at a finite Knudsen number exhibits a temperature jump at the wall. This means that the temperature of gas molecules that collide with the wall and the temperature of the wall are not the same. Noticing that in the diffuse boundary conditions the reflected gas molecules are modeled by the Maxwellian distribution function at the wall temperature and the colliding molecules are distributed very close to a Maxwellian but have a different temperature, the diffusion boundary conditions force the solution to form a discontinuity at the wall at $u = 0$. Thus high gradients will appear in the direction of the velocity variable near the wall at point $u = 0$. These gradients propagate inside the domain and decay quickly with a rate governed by the collision frequency $\nu(x, t)$. This in turns creates high gradients in the x direction, which produce a high frequency error in the solution.

The fact that the cold boundary has a higher density and thus effectively a higher collision frequency explains why more oscillations are observed near the cold wall than near the hot wall.

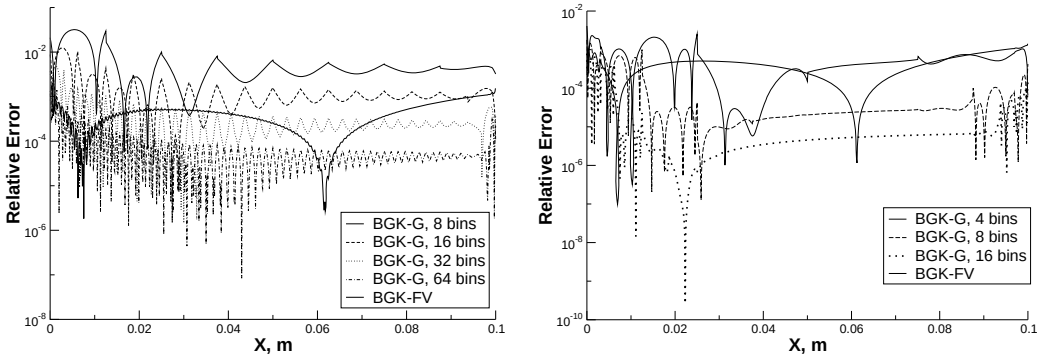

(a) (b)

FIGURE 7. Convergence of density in a Kn=0.01 heat transfer problem as a function of the number of cells. Comparison of (a) first degree and (b) fourth degree polynomial DG discretizations.

Let us now compare the macroparameters obtained by the FV and DG methods of discretization. The ratios of the FV temperature profiles to the corresponding reference DG solution computed using the ninth order in velocity and fifth order in physical space scheme are presented in Figure 8(a) for Kn=1. The figure shows that the FV solution has converged with respect to the number of spatial cells, since the solution does not change when the number of cells is increased from 100 to 300. However, there still is a difference between the FV and DG results that is related to the finite number of velocity bins used in the FV scheme (in this case, $(40, 30, 30)$). The FV scheme corresponds to the discrete ordinate approach on a uniform velocity grid and, as in low order DG schemes (see Figure 6), requires a very large number of velocity bins to achieve convergence better than in the second digit. The main reason for the inability of the FV method to accurately capture the temperature profile for a limited number of velocity bins is primarily related to the discontinuity of the velocity distribution function similar to that mentioned earlier. For the relatively high Knudsen number that we have used, the distribution function at any given spatial location represents a combination of two half-Maxwellians that correspond to particles reflected on the cold and hot plates. A large number of velocity bins is needed in the FV method in order to properly capture such a discontinuous shape.

Another important metric of accuracy of the obtained solution is the flow velocity between the plates. In the absence of plate motion, the gas bulk velocity should be zero at any point between the plates. The values of average gas velocity in the direction perpendicular to the plates are given in Figure 8(b) for the FV and DG approaches. The FV approach that uses 100 spatial cells is characterized by relatively high, on the order 0.1 m/s, velocities in the regions near the walls. The flow in the central region also has noticeable velocities, with gas moving at speeds about 0.002 m/s from the hot

to the cold wall. Magnitudes of the flow velocities are relatively small compared to the thermal velocity of about 350 m/s. However, these magnitudes may be considerably high for some low-speed microscale flow applications. The increase in the number of cells from 100 to 300 allowed a significant reduction of flow velocities, although they are still visible both in the central region and especially near the walls. It is interesting to note that this numerical effect, associated with the boundary condition specification in the FV method, is observed both at the cold and at the hot wall; the error near the cold wall is somewhat higher. For the DG discretization, the error in the flow velocity calculation is on the order of 10^{-5} m/s, and therefore is not visible in the figure (the DG result appears to be a straight line at $U_x = 0$).

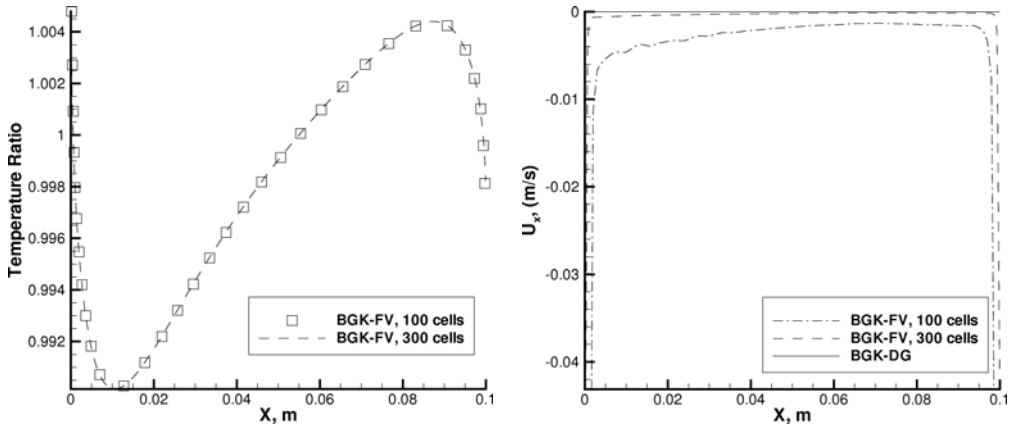

(a) (b)

FIGURE 8. FV to DG temperature ratio (a) and gas flow velocity (b), for heat transfer problem at Kn=1.

The decrease in the Knudsen number from 1 to 0.01 results in a significantly faster collisional relaxation of the distribution function, which is close to the Gaussian shape. A smaller number of velocity bins is therefore needed in the FV method to accurately describe the flow. This is clearly seen in Figure 9(a), where the ratios of the FV to DG temperature profiles are shown. At the same time, more spatial cells are required to properly capture the flow gradients. When 100 cells were used, the error was over one percent. This is not surprising since the cell size on the order of the gas mean free path is not expected to produce accurate results in this low order scheme. For the case of 1000 cells the error was significantly smaller and was less than 0.5% even near the cold surface where the error was largest. For further error reduction, more velocity bins are needed than the used value of (40,30,30). However, as was mentioned above, the accuracy of the FV approach is limited by the approximations used for the boundary conditions applied at the wall.

The issue with the boundary conditions is illustrated in Figure 9(b). For the DG discretization, the flow velocity is fairly close to zero, although the error is somewhat larger than for Kn = 1. As discussed earlier, the most noticeable error for this method is observed near the cold surface, where the magnitude of the flow velocity amounts to about 0.005 m/s. In the rest of the computational domain it is on the order of 10^{-4} m/s. The error was considerably larger for the FV method, even when 1000 cells

were used; in this case the cell size was about 10% of the gas mean free path. Note that the error in flow velocity was not localized near the walls, but propagated into the central region of the domain, where it was over two orders of magnitude larger than in the DG approach. The error was even larger for 100 cells, where it reached values in excess of 1 m/s.

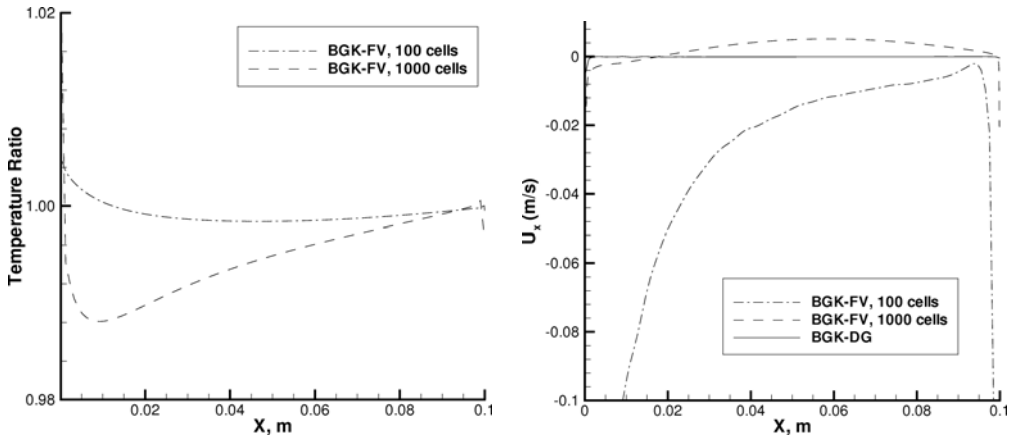

(a) (b)

FIGURE 9. FV to DG temperature ratio (a) and gas flow velocity (b), for heat transfer problem at Kn=0.01.

Analysis of transient flow evolution for the heat transfer problem was also conducted. At several time moments, the FV and DG results were compared for the two Knudsen numbers under considerations. The results were found to agree, with an error close to that observed for the steady state calculations presented earlier.

6. CONCLUSIONS

High order discontinuous Galerkin discretizations both in spatial and velocity variables were applied to the BGK equation. The normal shock wave and the heat transfer between parallel plates were analyzed in detail. It was found that the solutions to the normal shock wave problem exhibit very fast convergence with respect to the resolution in the velocity variable. The convergence of the solutions with respect to spatial variable corresponds to the order of polynomial interpolation. Furthermore, it was found that high order DG discretizations of the kinetic equations conserve mass, momentum and energy to a high precision. The DG solutions were compared to solutions obtained by a FV conservative technique and were found to be in excellent agreement. High order discretizations in the velocity variable, such as those using basis polynomials of eighth degree, were found to produce results not sensitive to the roughness in the solution.

It has been observed, however, that the solutions to the heat transfer problem do not exhibit a proper convergence rate with respect to the spatial variable. The solutions computed using approximations by polynomials of first and fourth degrees converge with the second order or more slowly. Loss of convergence in the heat transfer problem is attributed to the diffuse boundary conditions. It appears that a standard formulation

of the DG method is not well suited to handle the discontinuity at the boundary that is intrinsic to diffuse boundary conditions. Development of an improved DG techniques that handles such a discontinuity is therefore necessary.

7. Acknowledgments

The authors thank Prof. D. Arnold for insightful discussions of fast convergence of quadrature formulas and for his interest in this work. The authors are thankful to Prof. L.L. Foster for her help in the preparation of the final version of the manuscript. The first author was supported by the 2009 Air Force Summer Faculty Fellowship Program.

References

[1] S.M. Yen, Numerical solution of the nonlinear Boltzmann equation for nonequilibrium gas flow problems, *Annu. Rev. Fluid Mech.* Vol.16 (1984) pp. 67–97.

[2] B.J. Alder, T.E. Wainwright, Molecular dynamics by electronic computers, in: I. Prigogin (Ed.), *Transport Processes in Statistical Mechanics*, Interscience, New York, 1958, pp. 97–131.

[3] G.A. Bird, *Molecular Gas Dynamics and the Direct Simulation of Gas Flows*, Clarendon Press, Oxford, 1994.

[4] J. Fan, C. Shen, Statistical simulation of low-speed undirectional flows in transitional regime, in: *Pros. of 21st Symp. on Rarefied Gas Dynamics*, 1998, pp. 245–252.

[5] Q. Sun, I.D. Boyd, J. Fan, Development of an Information Preservation Method for Subsonic, Micro-Scale Gas Flows, in: T.J. Bartel, M.A. Gallis (Eds.), *Pros. of 22nd Rarefied Gas Dynamics Symposium*, July 2000, Sydney, Australia.

[6] C.R. Kaplan, E.S. Oran, Nonlinear filtering for low-velocity gaseous microflows, in: *Proc. of 23nd Symp. on Rarefied Gas Dynamics*, 2001, pp. 472–479.

[7] J. Chun, D.L. Koch, A direct simulation Monte Carlo method for rarefied gas flows in the limit of small Mach numbers, *Phys. Fluids* Vol. 17 (2005).

[8] P.L. Bhatnagar, E.P. Gross, M. Krook, A model for collision processes in gases I: Small amplitude processes in charged and neutral one-component systems, *Phys. Rev.*, Vol. 94 (1954) pp. 511–525.

[9] L.H. Holway, Numerical solutions for the BGK-model with velocity dependent collision frequency, in: *Rarefied Gas Dynamics, Vol.1 (Proceedings of Fourth International Symposium, University of Toronto, Toronto, 1964*, New York Academic Press, 1966, pp. 193–215.

[10] A.A. Alexeenko, S.F. Gimelshein, E.P. Muntz, A.D. Ketsdever, Kinetic modeling of temperature-driven flows in short microchannels, *Int. J. Thermal Sciences*, Vol. 45, No. 11 (2006) pp. 1045–1051.

[11] N. Selden, C. Ngalande, N. Gimelshein, S. Gimelshein, A. Ketsdever, A. Origins of radiometric forces on a circular vane with a temperature gradient, *J. Fluid. Mech.*, Vol. 634 (2009), pp. 419–431.

[12] L. Mieussens, Discrete-velocity models and numerical schemes for the Boltzmann-BGK equation in plane and axisymmetric geometries, *J. Comput. Phys.,* Vol. 162 (2000) pp. 429–466.

[13] G. May, B. Srinivasan, A. Jameson, Calculating three-dimensional transonic flow using a gas-kinetic BGK finite volume method, AIAA Paper 2005-1397.

[14] M. Ilgaz, I. Tuncer, Parallel implementation of gas-kinetic BGK scheme on unstructured hybrid grids, AIAA Paper 2006-3919.

[15] D.C. Wadsworth, N.E. Gimelshein, S.F. Gimelshein, I.J. Wysong, Assessment of translational anisotropy in rarefied flows using kinetic approaches, in: *Pros. of the 26th International Symposium on Rarefied Gas Dynamics*, AIP Conference Proceedings, Vol. 1084, 2008, pp. 206-211.

[16] N. Selden, N. Gimelshein, S. Gimelshein, A. Ketsdever, Experimental/computational approach to accommodation coefficients and its application to noble gases on aluminum surface, to appear in *Phys. Fluids*, Jan 2009.

[17] I.M. Gamba, J. Proft, Stable Discontinuous Galerkin Schemes for Linear Vlasov-Boltzmann Transport Equations, *ICES Report 07-25*, submitted for publication (2007).

[18] Y. Cheng, I.M. Gamba, A. Majorana, C.-W. Shu, A discontinuous Galerkin solver for Boltzmann Poisson systems in nano devices, to appear in *Comput. Methods. Appl. Mech. Eng.* (2009)

[19] A. Alexeenko, C. Galitzine, A.M. Alekseenko, High-order discontinuous Galerkin method for Boltzmann model equations, in: *AIAA Paper 2008-4256, 40th Thermophysics Conference*, Seattle, Washington, June 23-26, 2008.

[20] A. Alekseenko, Numerical properties of high order discrete velocity solutions to the BGK kinetic equation, submitted to *Applied Numerical Mathematics*, 2009.

[21] M.K. Gobbert, T.S Cale, A Galerkin method for the simulation of the transient 2-D/2-D and 3-D/3-D linear Boltzmann equation, *J. Sci. Comput.*, Vol. 30, No. 2 (2007) pp. 237–273.

[22] B. Cockburn, Discontinuous Galerkin methods for convection-dominated problems, in: T. Barth and H. Deconink (Eds.), *High-order methods for computational physics*, Springer-Verlag, Berlin, Vol. 9, *Lect. Notes Comput. Sci. Eng.*, 1999, pp. 69–224.

[23] B. Cockburn, C.-W. Shu, Runge-Kutta discontinuous Galerkin methods for convection-dominated problems, *J. Sci. Comput.*, Vol. 16, No. 3 (2001) pp. 173–261.